International Journal of Solids and Structures 257 (2022) 111592

Contents lists available at ScienceDirect

International Journal of Solids and Structures

journal homepage: www.elsevier.com/locate/ijsolstr

Rate-dependent wrinkling and subsequent bifurcations of an elastic thin film on a viscoelastic layer

Soham Mane, Rui Huang *

Department of Aerospace Engineering and Engineering Mechanics, University of Texas, Austin, TX 78712, United States

ARTICLE INFO

Keywords:
Wrinkling
Bifurcation
Thin film
Viscoelasticity

ABSTRACT

A trilayer model with a viscoelastic layer between an elastic thin film and a pre-stretched elastomer substrate is used to study the rate-dependent wrinkling and subsequent bifurcations, where the elastic film and the viscoelastic layer are compressed by releasing the pre-stretch of the substrate at a prescribed nominal strain rate. With a moderate substrate pre-stretch, the only bifurcation mode obtained is wrinkling, with evolution of wrinkle wavelength and amplitude depending on the strain rate and the thickness of the viscoelastic layer. With a relatively large pre-stretch, the wrinkles may evolve to advanced bifurcation modes. Localized ridge formation occurs when the strain rate is low and the viscoelastic layer is thin. In contrast, when the strain rate is relatively high and the viscoelastic layer is thick, period-doubling occurs after a critical strain, which may further evolve to period quadrupling and periodic folding by consecutive bifurcations. By varying the substrate pre-stretch and the thickness ratio, bifurcation phase diagrams at the end of compression are constructed for different nominal strain rates. After compression, holding the trilayer at a constant nominal strain allows the surface morphology to evolve over time, eventually reaching an equilibrium state independent of the strain rate. The equilibrium bifurcation phase diagram obtained after holding shows three bifurcation modes: wrinkling, ridge formation, and periodic folding. Compared to the elastic bilayer systems, the trilayer system with a viscoelastic mid-layer offers additional control parameters in terms of the nominal strain rate and the thickness ratio to induce various bifurcation modes, which may enable designing and producing desired features of surface morphology for novel applications.

1. Introduction

Surface wrinkling as a primary mode of bifurcation has been studied extensively in both homogeneous and layered materials (Biot, 1963; Allen, 1969). In particular, wrinkling of an elastic thin film on a soft substrate has been a prototypical model system, which has found a variety of applications, including stretchable electronics (Khang et al., 2006), multifunctional and smart surfaces (Chan et al., 2008; Lin et al., 2008; Rahmawan et al., 2010; Yang et al., 2010), and thin film metrology (Stafford et al., 2004; Chung, et al., 2011). If the substrate is elastic, linear or nonlinear, wrinkling is well understood with a critical strain and an equilibrium state, depending on the ratio between the elastic moduli of the film and the substrate (Huang et al., 2005; Jiang et al., 2007; Mei et al., 2011; Cao and Hutchinson, 2012). If the substrate is viscous or viscoelastic, wrinkling is a kinetic process and evolves over time (Huang and Suo, 2002; Huang, 2005; Huang and Im, 2006). Another type of substrate material considered is an inviscid liquid, in which case an equilibrium wrinkle wavelength was found to depend on the ratio between the bending modulus of the film and the mass density of the liquid (Pocivavsek et al., 2008; Brau et al., 2013).

More recent studies on surface instability have advanced towards other modes of bifurcation, such as creasing (Hong et al., 2009; Hohlfeld and Mahadevan, 2011; Cao and Hutchinson, 2011; Diab et al., 2013; Diab and Kim, 2014), period doubling (Brau et al., 2011; Sun et al., 2012; Cao and Hutchinson, 2012; Auguste et al., 2014; Zhao et al., 2015; Zhuo and Zhang, 2015; Cai and Fu, 2019), inward folding (Brau et al., 2013; Zhuo and Zhang, 2015), and ridge formation (Cao and Hutchinson, 2012; Ebata et al., 2012; Cao et al., 2014; Jin et al., 2015; Auguste et al., 2018). Most of these studies have focused on the cases of an elastic bilayer with a thin film on a thick substrate, for which a primary bilayer Ruga-phase diagram was constructed by Zhao et al. (2015 and 2016). A different set of phase diagrams were constructed by Wang and Zhao (2014) to predict both the initial and advanced modes of instabilities in compressed film-substrate systems, including wrinkles, creases, period

* Corresponding author.
E-mail address: ruihuang@mail.utexas.edu (R. Huang).

https://doi.org/10.1016/j.ijsolstr.2022.111592
Received 5 January 2022; Received in revised form 28 February 2022; Accepted 22 March 2022
Available online 24 March 2022

doubling, localized ridges, and buckle delamination. These studies have provided significant insights into the advanced modes of bifurcation beyond wrinkling and guided the design of bilayer material systems to achieve desired surface patterns for a wide variety of applications (Wang and Zhao, 2016).

In a recent experiment, both wrinkling and ridge formation were observed in a trilayer system with a thin elastic film and a highly viscous liquid layer on a pre-stretched elastomer substrate (Chatterjee et al., 2015). By releasing the pre-stretch of the elastomer substrate at a prescribed nominal strain rate, periodic wrinkles formed and evolved during compression. When a large pre-stretch was used, the wrinkles evolved to form tall ridges. The presence of the viscous liquid layer between the elastic film and the pre-stretched substrate introduced a material time scale, and the wrinkle evolution became rate dependent. Unlike the previous studies on wrinkling of an elastic film on a viscous or viscoelastic substrate (Huang and Suo, 2002; Huang, 2005; Huang and Im, 2006), the compressive strain in the film increased in the trilayer system as the pre-stretched substrate was released, and the compressive strain could be very large (up to 100%). While the effects of viscosity and viscoelasticity on wrinkling at small strains have been reasonably understood from the previous works, such effects on the advanced bifurcation modes beyond wrinkling have not received much attention. Zhao et al. (2016) noted that the material viscosity (if present) could lead to diverse modes of metastable configurations and enhance irreversibility with cyclic hysteresis in bilayer systems. Since polymeric materials are commonly used in experiments to develop wrinkles and advanced bifurcation modes, the effect of polymer viscoelasticity could be an important factor to be considered and explored. In the present study, we consider a trilayer system similar to that used in the experiments by Chatterjee et al. (2015), with a viscoelastic layer between an elastic thin film and a pre-stretched elastomer substrate (Fig. 1a). Our numerical simulations illustrate the effects of viscoelasticity on the evolution of wrinkles and advanced bifurcation modes (e.g., ridge formation and period doubling) in the trilayer system (Fig. 1, b-d).

The remainder of the paper is organized as follows. Section 2 summarizes the analytical predictions of the critical strain, wavelength and amplitude of wrinkling in elastic bilayers. Section 3 describes a finite element model to simulate wrinkling and subsequent bifurcations in the trilayer system. Results from the finite element simulations are discussed in Section 4, which are categorized in two subsections based on the substrate pre-stretch. Rate-dependent wrinkling is discussed first for the cases with a moderate pre-stretch, followed by advanced bifurcation modes for the cases with a relatively large pre-stretch. Based on the numerical simulations, we construct bifurcation phase diagrams at the end of compression as well as after holding for a long time to reach equilibrium. Section 5 concludes with a brief summary.

2. Analytical predictions for wrinkling

Previous works have developed a set of analytical solutions for wrinkling in elastic bilayer systems (Huang et al., 2005; Jiang et al., 2007; Mei et al., 2011; Cao and Hutchinson, 2012), which will be compared to numerical simulations of wrinkling in the trilayer system. For a sinusoidal wrinkle with a wavenumber k and an amplitude A, the elastic strain energy (per unit area) of the bilayer is (Huang et al., 2005):

$$U = U_0 + \frac{h_f \overline{E}_f}{4}\left(f - \varepsilon_f\right)k^2A^2 + \frac{h_f \overline{E}_f}{32}k^4A^4, \tag{1}$$

where U_0 is the elastic energy before wrinkling, ε_f is the compressive strain in the film before wrinkling, $\overline{E}_f = E_f/(1-\nu_f^2)$ is the plane-strain modulus of the film, h_f is the film thickness, and

$$f = \frac{1}{12}(kh_f)^2 + \frac{\overline{E}_s}{kh_f\overline{E}_f}g(kh_s, \nu_s), \tag{2}$$

$$g(kh_s, \nu_s) = \frac{(3-4\nu_s)\cosh(2kh_s) + 5 - 12\nu_s + 8\nu_s^2 + 2(kh_s)^2}{(6-8\nu_s)\sinh(2kh_s) - 4kh_s}, \tag{3}$$

with $\overline{E}_s = E_s/(1-\nu_s^2)$ as the plane-strain modulus of the substrate and h_s the substrate thickness

An equilibrium wrinkle wavenumber (k_{eq}) or wavelength ($\lambda_w = 2\pi/k_{eq}$) is selected by minimizing the elastic energy in Eq. (1), or equivalently by minimizing f in Eq. (2). The critical compressive strain for wrinkling is then obtained as $\varepsilon_{cr} = f_{min}$ with $k = k_{eq}$ in Eq. (2). Further minimizing the elastic energy with respect to the wrinkle amplitude predicts the equilibrium amplitude as.

$$A_w = \frac{2}{k_{eq}}\sqrt{\varepsilon_f - \varepsilon_{cr}}. \tag{4}$$

The predicted critical strain, equilibrium wrinkle wavelength and amplitude depend on the thickness ratio, h_s/h_f. For an infinitely thick substrate ($kh_s \gg 1$), they are predicted as (Huang et al., 2005):

$$\varepsilon_{cr} = \frac{1}{4}\left(\frac{3\overline{E}_s}{\overline{E}_f}\right)^{2/3}, \tag{5}$$

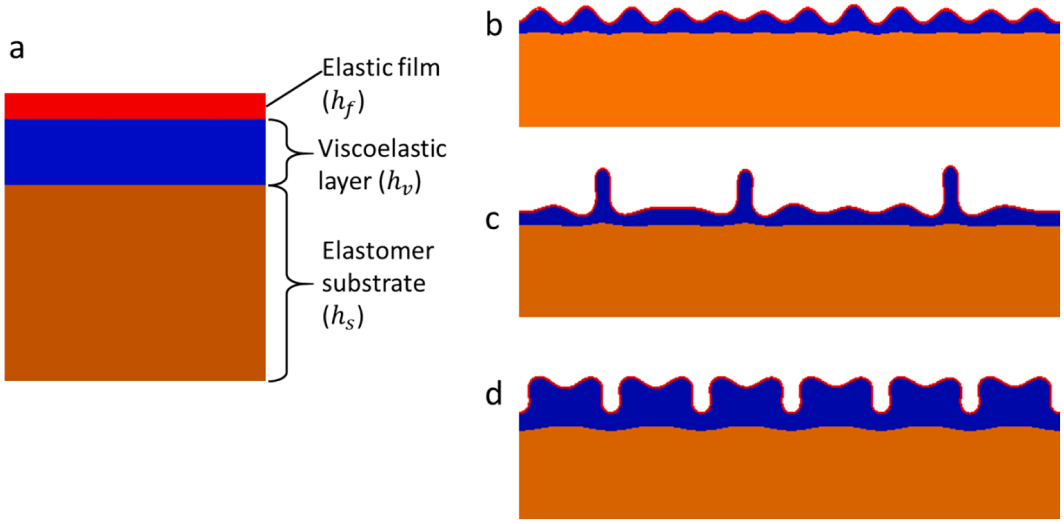

Fig. 1. (a) Schematic of a trilayer model, and simulated bifurcation modes: (b) wrinkling, (c) ridge formation, and (d) period doubling.

$$\lambda_w = 2\pi h_f \left(\frac{3\overline{E}_s}{\overline{E}_f}\right)^{-1/3}, \tag{6}$$

$$A_w = h_f \sqrt{\frac{\varepsilon_f}{\varepsilon_{cr}} - 1}. \tag{7}$$

On the other hand, if the substrate is thin ($kh_s \ll 1$) and incompressible ($\nu_s = 0.5$), the critical strain, wrinkle wavenumber and amplitude are predicted as (Huang et al., 2005):

$$\varepsilon_{cr} = \frac{h_f}{4h_s}\left(\frac{9\overline{E}_s}{4\overline{E}_f}\right)^{1/3}, \tag{8}$$

$$\lambda_w = 2\pi\sqrt{h_f h_s}\left(\frac{18\overline{E}_s}{\overline{E}_f}\right)^{-1/6}, \tag{9}$$

$$A_w = h_f \sqrt{\frac{1}{2}\left(\frac{\varepsilon_f}{\varepsilon_{cr}} - 1\right)}. \tag{10}$$

We note that Eqs. (8)–(10) were obtained by assuming a roller boundary condition at the bottom of the bilayer so that the bottom surface remains flat.

For the case with an elastic film on a viscoelastic layer, previous studies have predicted a fastest growing mode with a wrinkle wavelength depending on the pre-wrinkling strain or stress in the film (Huang, 2005; Huang and Im, 2006). In the present study, however, the strain in the film changes during compression with a nominal strain rate. As a result, the fastest growing mode is not uniquely defined. Rather, the wrinkle growth becomes strain rate dependent, with both the wavelength and amplitude evolving over time, different from the previous studies. At the limit of low or high strain rates, the viscoelastic layer may behave elastically with a rubbery or glassy modulus, in which case wrinkling may be predicted by the above analytical solutions for elastic bilayers with an effective elastic modulus of the substrate depending on the strain rate. Therefore, the rate-dependent wrinkling may be correlated to the rate-dependent effective modulus of the viscoelastic layer, as discussed further in Section 4.

3. Finite element model

We consider a trilayer system consisting of an elastic thin film lying on a viscoelastic layer of finite thickness (h_v), supported by a pre-stretched elastomer substrate (see Fig. 1a). The three layers are assumed to be perfectly bonded at the interfaces. While the elastomer substrate is pre-stretched to a prescribed stretch ($1.3 \leq \lambda_0 \leq 2$), the other two layers are assumed to be stress free as they are laid on top. Then, by releasing the elastomer substrate at a prescribed nominal strain rate, both the viscoelastic layer and the elastic film are compressed, leading to wrinkling (Fig. 1b) and subsequent bifurcations (Fig. 1, c and d). The presence of the viscoelastic mid-layer is essential for the rate-dependent behavior, and its thickness plays an important role in determining the advanced bifurcation modes (e.g., ridge formation or period doubling).

We employ two-dimensional (2D) finite element models to simulate the rate-dependent wrinkling and subsequent bifurcations in the trilayer system, using the commercial software ABAQUS (Simulia, Providence, RI, USA). The elastic film and the elastomer substrate are treated as hyperelastic by the neo-Hookean material model, while the viscoelastic layer is modeled as hyper-viscoelastic (HVE). The HVE model is a time-domain generalization of the hyperelastic constitutive model for finite-strain viscoelasticity (Simo, 1987). It is also a generalized Maxwell model of linear viscoelasticity by incorporating nonlinear geometry associated with large deformation, with hyperelastic limits for the short-term (glassy) and long-term (rubbery) behaviors. The time dependence is described by a Prony series with one intrinsic time scale (τ_v), which is used to normalize the time and strain rate in all simulations. The shear modulus of the substrate (μ_s) is set to be 1 after normalization, and the shear modulus of the film is normalized accordingly as $\mu_f/\mu_s = 200$. For the viscoelastic layer, the shear modulus at the rubbery limit is set to be: $\mu_r/\mu_s = 0.02$, and the glassy modulus is 10 times of the rubbery modulus ($\mu_g = 10\mu_r$). All three layers are assumed to be incompressible. This set of material properties are selected to illustrate the effects of viscoelasticity, focusing on the effects of the normalized strain rate ($\dot{\varepsilon}\tau_v$), the normalized viscoelastic layer thickness (h_v/h_f), and the pre-stretch of the substrate (λ_0).

All dimensions of the trilayer model are normalized with respect to the film thickness (h_f). Specifically, the length of the substrate before pre-stretch is set to be: $L/h_f = 500$, and the substrate thickness is: $h_s/h_f = 70$; both are chosen to be sufficiently large for the numerical results to be insensitive to the particular values. The effect of the viscoelastic layer thickness is investigated by varying the thickness ratio h_v/h_f from 5 to 120.

The symmetry boundary conditions are applied at the left boundary of the domain, while a prescribed velocity in the negative x direction is imposed on the right boundary to simulate a nominal compressive strain rate, $\dot{\varepsilon} = |\dot{u}|/(\lambda_0 L)$, as the elastomer substrate contracts, compressing the top two layers. A roller boundary condition is assumed along the bottom of the substrate, and the top surface of the film is traction free. With these boundary conditions, we ignore the effect due to free edges of the film in the experiments (Chatterjee et al., 2015) and focus on the region far away from the edges (assuming a long film). The edge effects may be estimated by a shear-lag type analysis as in previous studies (Chatterjee et al., 2015; Liang et al., 2002).

Assuming plane strain conditions, the 2D hybrid elements (CPE4H) are used to discretize all three layers. Structured meshes are used for the film and the viscoelastic layer with four rectangular elements across the film thickness and 1000 elements along the length, while an unstructured mesh with quadrilateral elements is used for the elastomer substrate. Since the substrate undergoes nearly homogenous deformation, we can afford to use a relatively coarse mesh without compromising the accuracy of the numerical results. A numerical convergence study was performed to select appropriate element size and mesh. The dynamic implicit analysis is conducted for time evolution with adaptive time increments. In all simulations, the kinetic energy is small compared to the strain energy so that the behavior is considered quasi-static. To simulate wrinkling and subsequent bifurcations, small imperfections are introduced in the finite element model using the first 20 eigen modes from a linear eigenvalue analysis of the trilayer model.

The finite element simulation follows in 4 steps: (1) Pre-stretching of the elastomer substrate; (2) Activation of the elastic film and the viscoelastic layer on top of the substrate; (3) Compressing the top two layers by releasing the pre-stretch of the substrate at a prescribed nominal strain rate; (4) Holding the trilayer system at a constant nominal strain. The substrate pre-stretch varies from moderate ($\lambda_0 = 1.3$) to large ($\lambda_0 = 2.0$). The compression step stops when the stretch of the substrate reaches 1.2. The nominal strain at the end of the compression step is: $\varepsilon_f = (\lambda_0 - 1.2)/\lambda_0$, which varies from 0.077 to 0.4, similar to the strains recorded in the experiments (Chatterjee et al., 2015).

4. Results and discussion

4.1. Wrinkling with a moderate pre-stretch

With a moderate pre-stretch ($\lambda_0 = 1.3$), wrinkling of the elastic film starts to grow at a critical compressive strain, and both the wrinkle wavelength and amplitude continue to evolve during compression, as observed in experiments (Chatterjee et al., 2015). Unlike the elastic bilayer systems in many previous works (Huang et al., 2005; Mei et al., 2011; Cao and Hutchinson, 2012), the critical strain, wrinkle wavelength and amplitude all become rate dependent in the trilayer model with a viscoelastic mid-layer, as discussed here based on numerical simulations.

4.1.1. Critical strain

It can be challenging to precisely identify the time or strain level at which wrinkles start to grow in the experimental setup (Chatterjee et al., 2015), especially at relatively high strain rates. In our finite element simulations, the critical strain for wrinkling can be determined more accurately as it is only limited by the numerical strain increment. One way to determine the critical strain is based on the wrinkle amplitude. However, with initial imperfections, the wrinkle amplitude grows smoothly in the numerical simulation (see Fig. 5), which makes it difficult to identify the critical strain. Alternatively, the horizontal reaction force at the right edge of the elastic film deviates from a simple homogeneous solution once wrinkling starts, as shown in Fig. 2a. This deviation offers a convenient way to determine the critical strain for onset of wrinkling. It is found that the critical strain depends on the normalized strain rate, $\dot{\varepsilon}\tau_v$, and the thickness ratio, h_v/h_f, as shown in Fig. 2b. At a relatively high strain rate ($\dot{\varepsilon}\tau_v = 1$), the critical strain is in close agreement with the predicted critical strain for an elastic bilayer system with a substrate layer corresponding to the glassy state of the viscoelastic layer. At a relatively low strain rate ($\dot{\varepsilon}\tau_v = 5 \times 10^{-4}$), the critical strain is lower but remains higher than the predicted critical strain for an elastic bilayer with a substrate layer corresponding to the rubbery state of the viscoelastic layer. Our simulations could not reach the predicted critical strain at the rubbery limit for the lowest strain rate considered ($\dot{\varepsilon}\tau_v = 5 \times 10^{-4}$), which may be attributed to the presence of the elastomer substrate underneath the viscoelastic layer in the trilayer model. The effect of the substrate is more significant at the rubbery limit because the viscoelastic layer is more compliant ($\mu_r/\mu_s = 0.02$) than at the glassy limit ($\mu_g/\mu_s = 0.2$). Nevertheless, the onset of wrinkling in the trilayer system is slightly delayed (in terms of the compressive strain) as the nominal strain rate increases, which can be related to the rate-dependent effective stiffness of the viscoelastic layer.

4.1.2. Wrinkle wavelength

To determine the wrinkle wavelength, we take a discrete Fourier transform of the film deflection at the end of the compression step to find the dominant mode. It is found that the wrinkle wavelength depends on the normalized strain rate, $\dot{\varepsilon}\tau_v$, and the thickness ratio, h_v/h_f, as shown in Fig. 3. At a relatively high strain rate ($\dot{\varepsilon}\tau_v = 1$), the wrinkle wavelength is in close agreement with the predicted wavelength for an elastic bilayer with a substrate layer corresponding to the glassy state of the viscoelastic layer. At a low strain rate ($\dot{\varepsilon}\tau_v = 5 \times 10^{-4}$), the wrinkle wavelength is longer but remains shorter than the predicted wavelength for an elastic bilayer system with a substrate layer corresponding to the rubbery state of the viscoelastic layer. Again, our simulations could not reach the predicted wavelength at the rubbery limit for the lowest strain rate considered ($\dot{\varepsilon}\tau_v = 5 \times 10^{-4}$), likely due to the presence of the elastomer substrate in the trilayer model.

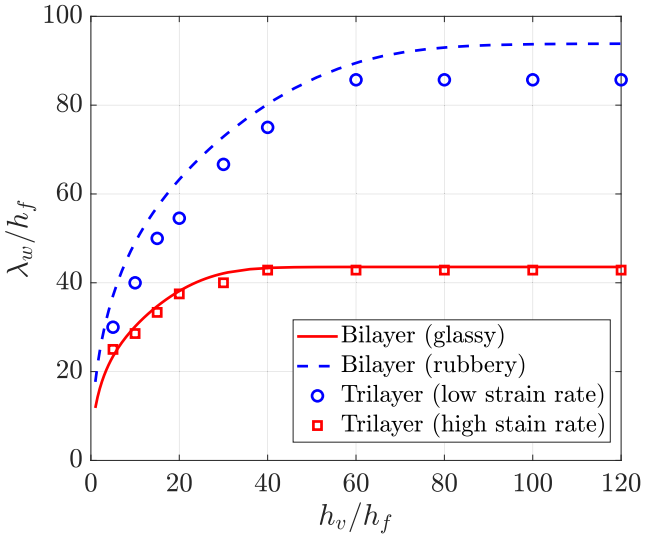

Fig. 3. Wrinkle wavelength versus the thickness ratio, at low and high strain rates ($\dot{\varepsilon}\tau_v = 5 \times 10^{-4}$ and 1), in comparison with the wrinkle wavelength for an elastic bilayer system predicted by Eqs. (1–3) using either the glassy or rubber modulus of the viscoelastic layer.

The wrinkle wavelengths for various combinations of the nominal strain rate and the thickness ratio are shown in Fig. 4. For each thickness ratio (h_v/h_f), a viscoelastic transition can be seen from a relatively short wavelength at the highest strain rate to a relatively long wavelength at the lowest strain rate. The transition occurs over a range of strain rate from $\dot{\varepsilon}\tau_v \sim 10^{-3}$ to 10^{-1} for all thickness ratios, whereas the transition is more pronounced for larger thickness ratios. The transition in wavelength appears to be not smooth, partly because multiple wrinkle modes may co-exist during transition and only one of them with the maximum amplitude is taken as the dominant mode. The dependence of the wrinkle wavelength on the thickness ratio is similar to that predicted for elastic bilayers (Fig. 3), with a rate-dependent effective stiffness for the viscoelastic layer. For $h_v/h_f \geq 80$, the wrinkle wavelength becomes nearly independent of the thickness ratio at both high and low strain rates, although different wavelengths may appear during the transition at intermediate strain rates. Nevertheless, the rate-dependent wrinkle wavelength can in principle be correlated to the viscoelastic property of the mid-layer in the trilayer system. It is thus possible to deduce the viscoelastic property of a thin layer by measuring the rate-dependent wrinkle wavelength with a thinner elastic film on top. Similar applications of wrinkling for material metrology have been explored previously

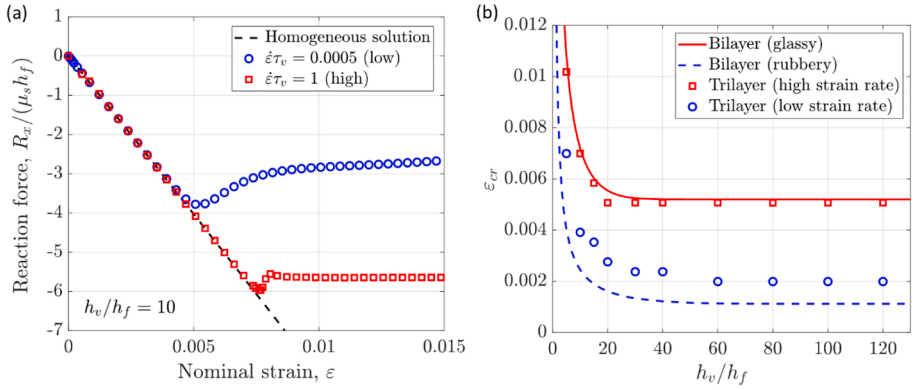

Fig. 2. (a) Horizontal reaction force at right edge of the film versus the nominal compressive strain, at two different strain rates ($\dot{\varepsilon}\tau_v = 5 \times 10^{-4}$ and 1); (b) Critical strain for onset of wrinkling versus the thickness ratio, in comparison with the critical strain for an elastic bilayer system predicted by Eqs. (1–3) using either the glassy or rubber modulus of the viscoelastic layer.

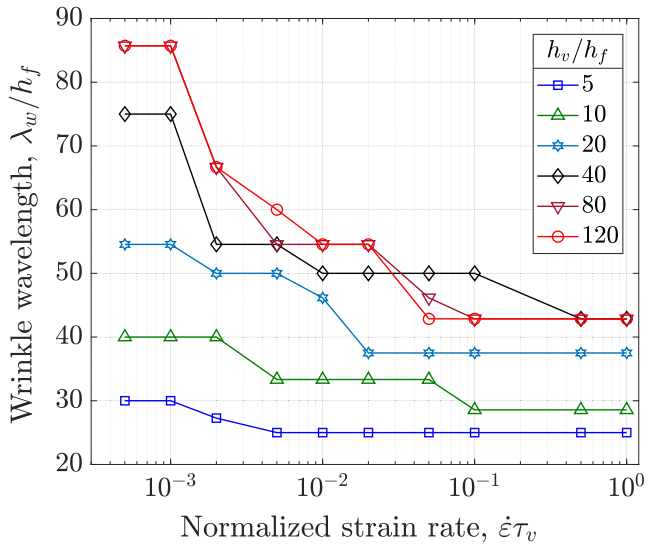

Fig. 4. Wrinkle wavelength at the end of compression versus the nominal strain rate, for different thickness ratios.

for both elastic and viscoelastic thin films (Stafford et al., 2004 and 2006; Chan et al., 2009; Chung et al., 2011).

4.1.3. Wrinkle amplitude

Fig. 5 shows the evolution of wrinkle amplitude as the nominal compressive strain increases at different strain rates. The wrinkle amplitude is calculated by the root-mean-square (RMS) average of the film deflection (Huang and Im, 2006). The numerical results are largely bounded in between the two elastic limits for bilayers, as predicted by Eq. (4) with an elastic substrate corresponding to the glassy or rubbery state of the viscoelastic layer. At a relatively high strain rate ($\dot{\varepsilon}\tau_v = 1$), the wrinkle amplitude closely follows the predicted amplitude with the glassy modulus of the viscoelastic layer. At a lower strain rate, however, the wrinkle amplitude deviates from the elastic prediction at the glassy limit and shifts up toward the elastic prediction at the rubbery limit. This indicates a transition in the wrinkling mode during compression, and the transition strain depends on the nominal strain rate. At the lowest strain rate considered ($\dot{\varepsilon}\tau_v = 5 \times 10^{-4}$), the wrinkle amplitude remains below the rubbery limit for $h_v/h_f = 10$ (Fig. 5a), but becomes closer to the rubbery limit for a thicker viscoelastic layer with $h_v/h_f = 80$ (Fig. 5b). This suggests that the presence of an elastomer substrate in the trilayer system has a strong influence on the wrinkles at the low strain rate, especially for a relatively thin viscoelastic layer, but the effect is reduced for a relatively thick viscoelastic layer.

The wrinkle amplitudes at the end of compression (with $\varepsilon_f = 0.077$) for different strain rates and different thickness ratios are shown in Fig. 6. Similar to the wavelengths in Fig. 4, for each thickness ratio, a viscoelastic transition can be seen from a relatively small amplitude at the highest strain rate to a relatively large amplitude at the lowest strain rate. The transition occurs over a range of strain rates from $\dot{\varepsilon}\tau_v \sim 10^{-3}$ to 10^{-1}, and the transition is more prominent for the cases with relatively large thickness ratios. Therefore, both the wavelength and amplitude of wrinkling are rate dependent in the trilayer system, due to the viscoelastic mid-layer.

After the compression step, the wrinkles may continue to evolve while the trilayer is held at a constant nominal strain ($\varepsilon_f = 0.077$). After a sufficiently long time, the wrinkles approach an equilibrium state, independent of the strain rate used in the compression step. Similar to previous studies on wrinkling of an elastic thin film on a viscoelastic substrate (Huang, 2005; Huang and Im, 2006), both the wrinkle wavelength and amplitude increase over time during holding. However, the presence of the pre-stretched elastomer substrate in the trilayer model may affect the wrinkles so that the equilibrium wrinkle wavelength and amplitude may differ from the predictions for the elastic bilayer systems. In the case of a very thin viscoelastic layer (e.g., $h_v/h_f = 5$), the wrinkles may evolve to form localized ridges after holding. The ridge formation is an advanced bifurcation mode as discussed next.

4.2. Bifurcation modes beyond wrinkling

By increasing the pre-stretch of the substrate, the film is subject to a higher compressive strain (up to $\varepsilon_f = 0.4$) and the wrinkles may evolve to different bifurcation modes. Here we use the finite element model to

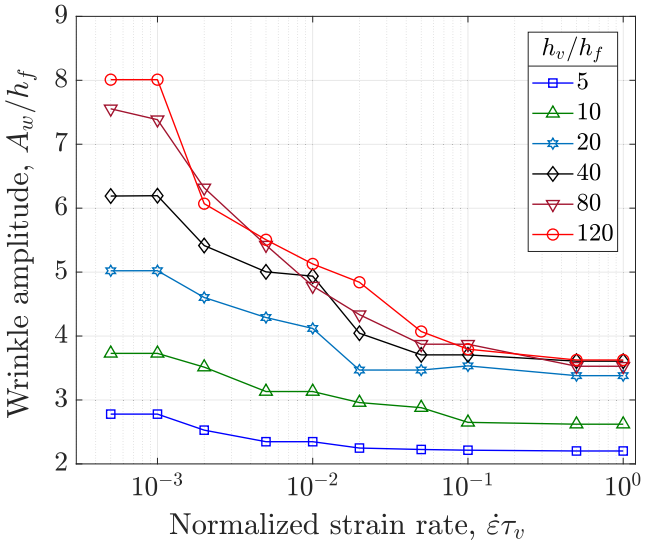

Fig. 6. Wrinkle amplitude at the end of compression versus the nominal strain rate, for different thickness ratios.

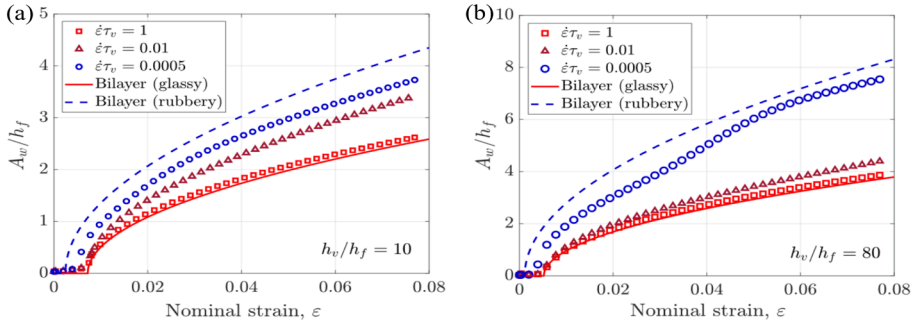

Fig. 5. Evolution of wrinkle amplitude as a function of the nominal compressive strain at different strain rates, for two different thickness ratios: (a) $h_v/h_f = 10$ and (b) $h_v/h_f = 80$.

simulate the subsequent bifurcation modes of the tri-layer system with pre-stretches ranging from 1.4 to 2. In all cases, we stop the compression step when the substrate stretch is down to 1.2. By varying the nominal strain rate ($\dot{\varepsilon}\tau_v$) and the thickness ratio (h_v/h_f), different bifurcation modes are obtained and discussed as follows.

4.2.1. Ridge formation

With a relatively high pre-stretch, a low strain rate, and a small thickness ratio, our simulations show that the trilayer system develops localized ridges (Fig. 1c) following the initial wrinkling. Fig. 7 shows the evolution of the surface profile as the nominal strain increases, with $\lambda_0 = 1.6$, $h_v/h_f = 5$, and $\dot{\varepsilon}\tau_v = 0.001$. At a relatively small strain ($\varepsilon = 0.116$), sinusoidal wrinkles are prominent over the surface, with nearly uniform wrinkle amplitude. At a larger strain ($\varepsilon = 0.177$), the wrinkles become less uniform, with some peaks growing higher than others. As the strain increases further, the growth of the higher peaks flattens the lower wrinkles nearby. At the end of compression ($\varepsilon_f = 0.25$), we obtain a few tall ridges separated by relatively flat regions with small wrinkles. Similar ridge formation was observed previously in experiments (Chatterjee et al., 2015; Cao et al., 2014; Auguste et al., 2018). Unlike the wrinkle-ridge transition in an elastic bilayer system, which was found to be a discontinuous snap transition (Jin et al., 2015; Takei et al., 2014), the wrinkle-ridge transition in the trilayer model appears to be a continuous process, possibly due to the presence of a viscoelastic mid-layer. A continuous ridge formation was also observed in an experiment with a glassy polymer film on an elastomeric substrate (Ebata et al., 2012).

To describe the ridge formation, we define three geometric parameters (see inset of Fig. 8): the ridge height (A_r) is the vertical distance between the peak and base of each ridge, the ridge width (b_r) is the horizontal distance between the two bases of each ridge, and the ridge

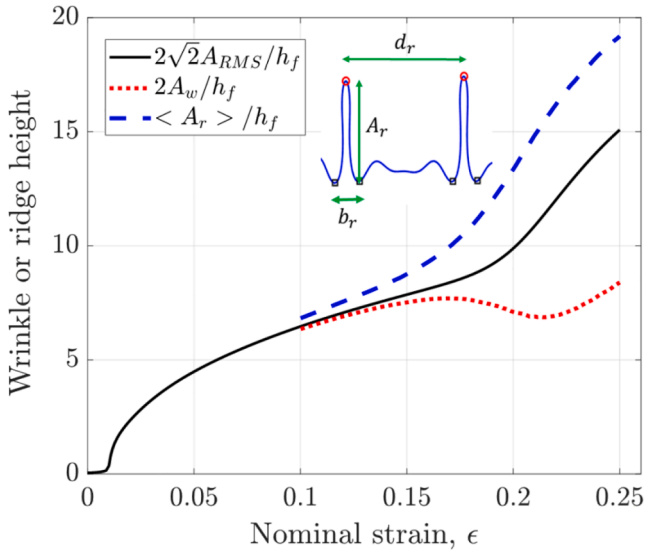

Fig. 8. Evolution of the wrinkle and ridge height in a trilayer system with $\lambda_0 = 1.6$, $h_v/h_f = 5$, and $\dot{\varepsilon}\tau_v = 0.001$. The inset shows the ridge geometry, where the peaks and bases are demarcated with red circle and black squares, respectively.

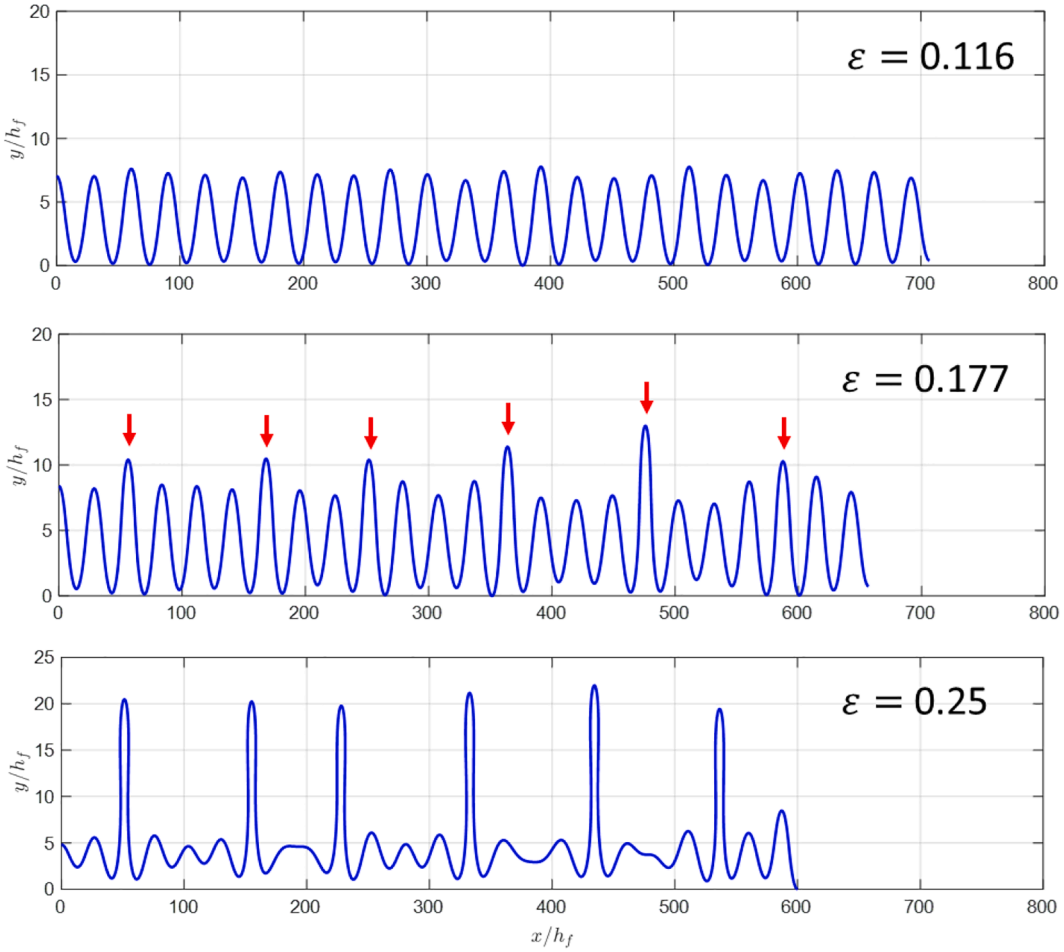

Fig. 7. Evolution of the film surface profile in a trilayer model at different nominal strains, with $\lambda_0 = 1.6$, $h_v/h_f = 5$, and $\dot{\varepsilon}\tau_v = 0.001$.

spacing (d_r) is the horizontal distance between the peaks of adjacent ridges. Fig. 8 shows the evolving wrinkle amplitude and ridge height in the trilayer model with $\lambda_0 = 1.6$, $h_v/h_f = 5$, and $\dot{\varepsilon}\tau_v = 0.001$. For nearly uniform wrinkles, the RMS of the film deflection is proportional to the average wrinkle amplitude, $A_w = \sqrt{2}A_{RMS}$. To compare with the ridge height, we plot $2\sqrt{2}A_{RMS}$ as a function of the nominal strain, which shows the onset of wrinkling at a small strain (~0.01). The average ridge height for the 6 ridges in Fig. 7 is shown to grow faster after the nominal strain exceeds 0.1. Meanwhile, the RMS amplitude of the regions between the ridges grows slower and even decreases. The onset of the secondary bifurcation occurs at a nominal strain of ~ 0.1, much higher than the critical strain for wrinkling. A similar critical strain for ridge formation was observed in an experiment with a stiff PDMS layer on a pre-stretched soft PDMS substrate (Jin et al., 2015). As the ridge height grows, the ridge width decreases with increasing nominal strain. As a result, the aspect ratio of the ridges (A_r/b_r) increases from around 0.3 to nearly 1. Meanwhile, the ridge spacing also decreases as the nominal strain increases. It is found that the initial ridge spacing is roughly three to four times of the wrinkle wavelength, as shown in Fig. 7. Thus, one out of every three or four wrinkle peaks grows to form localized ridges, similar to the formation of wrinkle-creases in R. Zhao et al. (2015), where every four other wrinkle valleys make setback creases.

With a larger pre-stretch and hence a larger compressive strain, additional ridge formation is possible in the trilayer model after formation of the first set of ridges. As shown in Fig. 9 for $\lambda_0 = 2$, $h_v/h_f = 5$, and $\dot{\varepsilon}\tau_v = 0.001$, while a set of seven primary ridges have formed at $\varepsilon = 0.28$, three new ridges appear at $\varepsilon = 0.375$. It is found that the height of the first set of ridges is limited and remains nearly constant after $\varepsilon = 0.28$. Further compression of the film promotes growth of new ridges, effectively reducing the average ridge spacing, as observed in previous experiments (Cao et al., 2014; Wang and Zhao, 2014). This phenomenon is analogous to channel cracking in thin films subject to tension, where parallel channel cracks may grow simultaneously first, followed by additional cracks growing in between (Xia and Hutchinson, 2000). A somewhat different progression in ridge formation was reported for an elastic bilayer under equi-biaxial compression (Takei et al., 2014), where the number of ridges increased continuously from one to six within the computational domain. The limited growth of the ridge height is similar to ridge localization in elastic bilayers as noted in previous studies (Takei et al., 2014; Zhao et al., 2015). The presence of a thin viscoelastic layer may simply regulate the wrinkle-ridge transition with little effect on the height limit.

After the compression step, the ridges largely remain unchanged while the trilayer is held at a constant nominal strain. In some cases the ridges may evolve back to wrinkles, typically when the ridges are not fully developed by the end of the compression, with a relatively small aspect ratio (A_r/b_r).

4.2.2. *Period doubling/quadrupling and folding*

With a relatively high pre-stretch, a high strain rate, and a large thickness ratio, our simulations show that the trilayer system develops period doubling (Fig. 1d) following the initial wrinkling. An example of the period doubling process is shown in Fig. 10, for a trilayer model with $\lambda_0 = 2$, $h_v/h_f = 10$, and $\dot{\varepsilon}\tau_v = 0.1$. With the relatively high strain rate, the wrinkles remain nearly uniform up to a fairly large strain ($\varepsilon = 0.32$), with no ridge formation. At $\varepsilon = 0.35$, period doubling starts to develop. By the end of compression ($\varepsilon_f = 0.4$), a period-doubling pattern is fully developed with alternating valley depths. Following the geometric

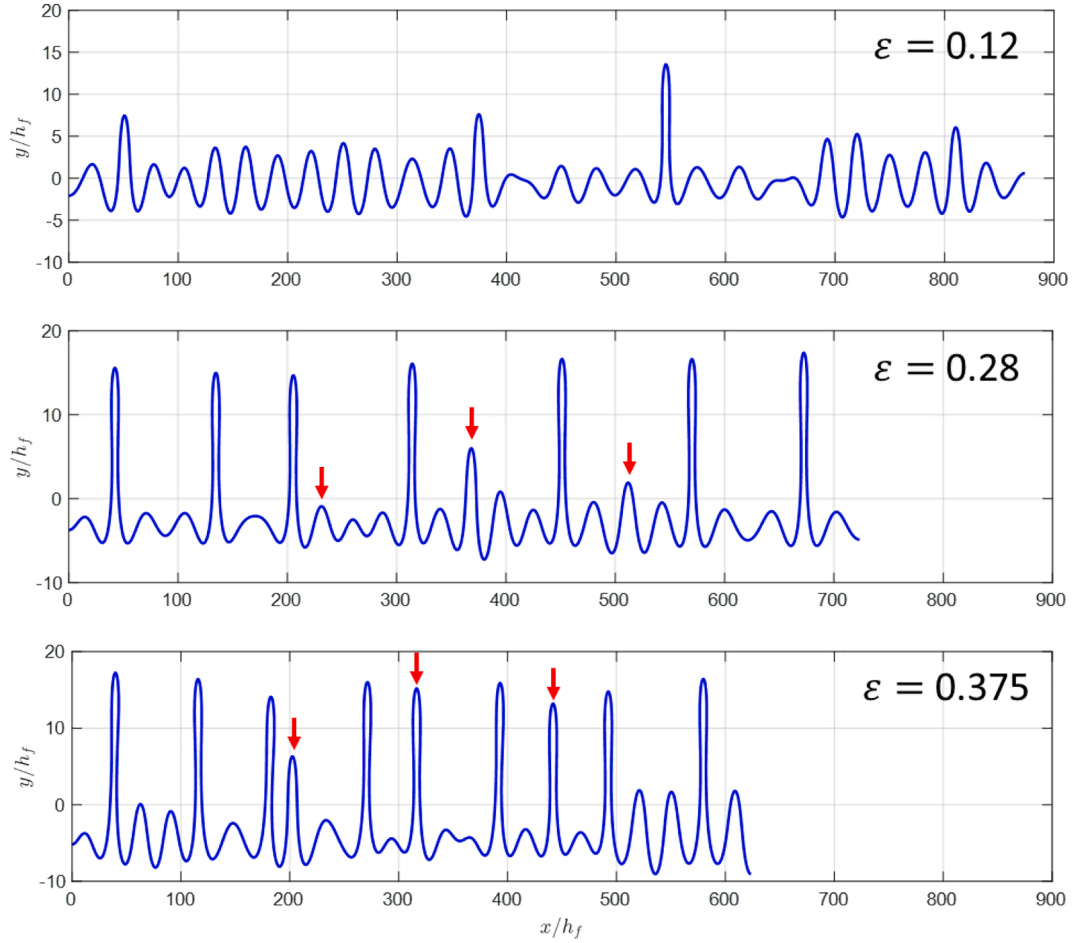

Fig. 9. Evolution of the film surface profile in a trilayer model at different nominal strains, with $\lambda_0 = 2$, $h_v/h_f = 5$, and $\dot{\varepsilon}\tau_v = 0.001$.

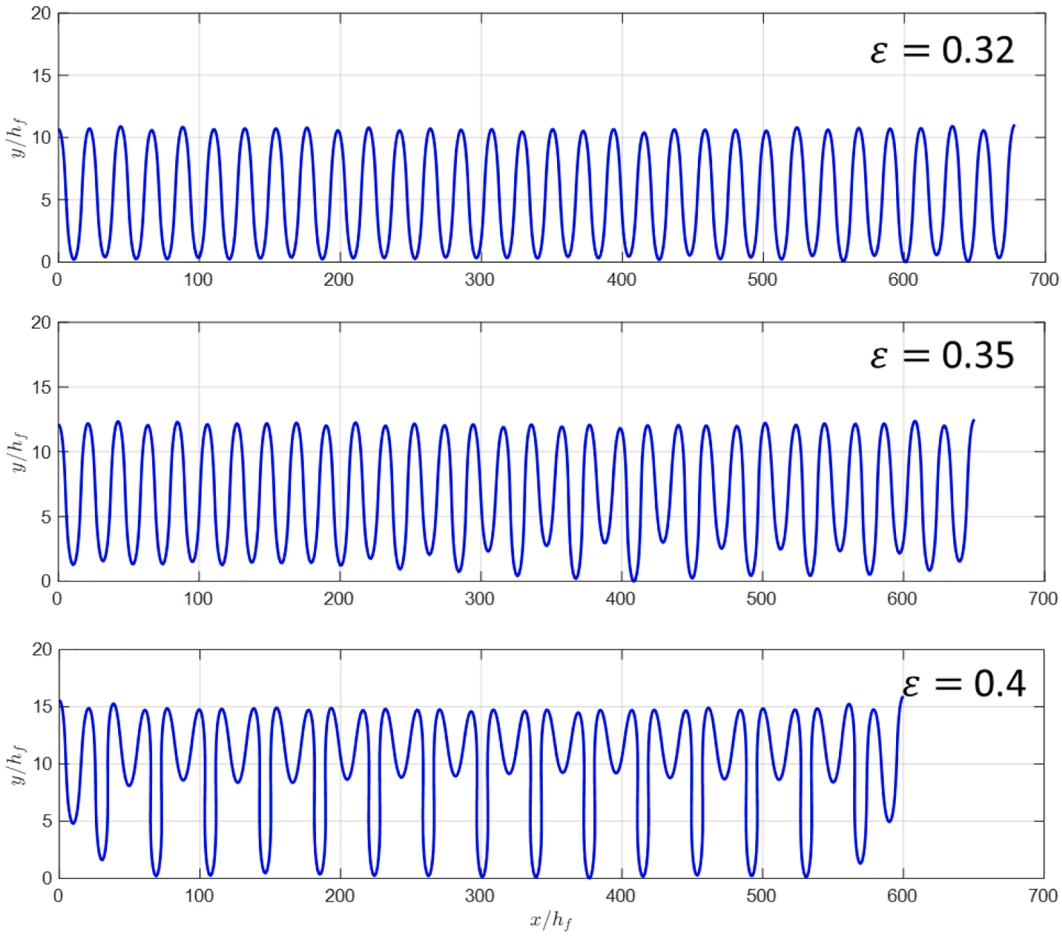

Fig. 10. Evolution of the film surface profile in a trilayer model at different nominal strains, with $\lambda_0 = 2$, $h_v/h_f = 10$, and $\dot{\epsilon}\tau_v = 0.1$.

description of period doubling in previous works (Brau et al., 2013; Zhao et al., 2016), let A_p be the primary valley depth and A_s be the secondary valley depth, as shown by the inset of Fig. 11. The evolution of the average valley depths is shown in Fig. 11. Before period doubling, we have nearly uniform wrinkles with $A_p = A_s$, which is twice of the wrinkle amplitude by definition. The onset of period doubling occurs at around $\varepsilon = 0.32$ as the two valley depths bifurcate into two branches, one increasing and the other decreasing. The critical strain for period doubling in this case is comparable to those predicted by Cao and Hutchinson (2012) for elastic bilayers with a pre-stretched substrate. Similar bifurcation diagrams for period doubling have been obtained previously for bilayer systems (Brau et al., 2011 and 2013; Auguste et al., 2014; Zhao et al., 2016; Budday et al., 2015).

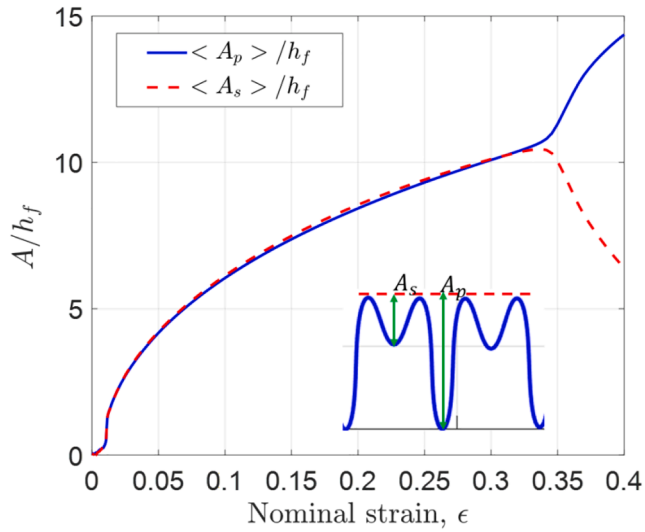

Fig. 11. Evolution of the average depths of the primary and secondary valleys as the nominal strain increases in a trilayer model with $\lambda_0 = 2$, $h_v/h_f = 10$, and $\dot{\epsilon}\tau_v = 0.1$. Inset shows the definition of the primary and secondary valley depths.

With a larger thickness ratio, the period doubling mode can further evolve to period quadrupling, as shown in Fig. 12a for $h_v/h_f = 80$, $\dot{\epsilon}\tau_v = 1$ and $\lambda_0 = 2$. In this case, frictionless self-contact is introduced for the elastic film in the finite element model, as period quadrupling leads to folding and self-contact of the film surface. The average depths of the primary and secondary valleys are shown in Fig. 12c, which shows clearly the consecutive bifurcations from wrinkling to period doubling and then to period quadrupling. Compared to Fig. 11, the onset of period doubling occurs at a smaller nominal strain (~0.19), which can be attributed to the reduced effect of the substrate pre-stretch with a thicker mid-layer.[1] Subsequently, the onset of period quadrupling occurs at a nominal strain of ~ 0.3, when the branch of the primary valley depth

[1] The critical strain for period doubling in elastic bilayers has been predicted to increase with increasing pre-stretch of the substrate (Cao and Hutchinson, 2012; Auguste et al., 2014; Y. Zhao et al., 2015; Zhuo and Zhang, 2015). For the trilayer model in the present study, the effect of substrate pre-stretch decreases with increasing thickness of the viscoelastic mid-layer, thus lowering the critical strain for period doubling.

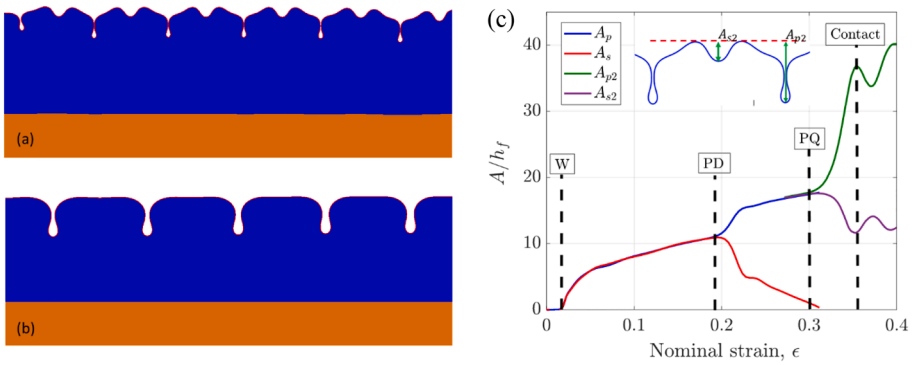

Fig. 12. (a) Period quadrupling at the end of compression, and (b) periodic folding (inward) after holding at a constant nominal strain ($\varepsilon_f = 0.4$), for a trilayer model with $h_v/h_f = 80$, $\dot{\epsilon}\tau_v = 1$, and $\lambda_0 = 2$. (c) Evolution of the average depths of the primary and secondary valleys defined in the inset. The onset of wrinkling (W), period doubling (PD), period quadrupling (PQ), and self-contact are indicated by vertical dashed lines.

(A_p) bifurcates to two branches (A_{p2} and A_{s2}). When the self-contact of the film surface occurs, the primary valley depth (A_{p2}) reaches a peak and decreases slightly before it grows further. Similar consecutive bifurcations have been observed in experiments (Brau et al., 2011) and simulated previously for elastic bilayers (Jung et al., 2015; R. Zhao et al., 2015).

It is found that the surface continues to evolve during holding at the constant nominal strain (e.g., $\varepsilon_f = 0.4$ for $\lambda_0 = 2$). After a sufficiently long time, period doubling may evolve back to wrinkles or grow to period quadrupling and then folding. There appears to exist a threshold for period doubling to grow further, depending on the ratio A_p/A_s. In the case of period quadrupling at the end of compression (Fig. 12a), the surface evolves to form periodic folding with a nearly flat surface between the folds, as shown in Fig. 12b. Here, the transition from period quadrupling to periodic folding is defined based on the secondary valley depth A_{s2}, which nearly vanishes (e.g., $A_{s2}/h_f < 1$) after holding for a long time ($t/\tau_v > 100$). The bifurcation pathway from wrinkling to folding through period doubling and quadrupling is similar to that in elastic bilayers predicted by R. Zhao et al. (2015). However, in the trilayer model, the period doubling and quadrupling patterns appear to be unstable upon holding, which may be attributed to two effects: (1) The presence of a pre-stretched elastomer substrate tends to stabilize periodic wrinkles against period doubling, especially for a relatively thin mid-layer, as observed in experiments with an elastic bilayer on a pre-stretched substrate (Auguste et al., 2018); (2) For a relatively thick mid-layer, period doubling evolves to periodic folding after holding, possibly due to the highly compliant mid-layer with a rubbery modulus $\mu_r/\mu_f = 10^{-4}$ in the present model.

We note that, because the behavior of a viscoelastic material is history dependent, the evolution of surface bifurcation is expected to be history dependent if the compression rate is not a constant. Here, motivated by the experiments in Chatterjee et al. (2015), we have considered the cases with constant rates and subsequent holding.

4.2.3. *Bifurcation phase diagrams*

Depending on the substrate pre-stretch (λ_0), the nominal strain rate ($\dot{\epsilon}\tau_v$), and the thickness ratio (h_v/h_f), different bifurcation modes are obtained in the trilayer model at the end of the compression step. We summarize our simulation results in bifurcation phase diagrams, as shown in Fig. 13. The boundary lines are drawn approximately between the cases with different bifurcation modes denoted by different symbols. At a relatively high strain rate ($\dot{\epsilon}\tau_v = 1$), we obtain three different modes: wrinkling (W), period doubling (PD), and period quadrupling (PQ). The PD and PQ modes are favored as the pre-stretch or the thickness ratio increases. In contrast, at a relatively low strain rate ($\dot{\epsilon}\tau_v = 0.01$), we obtain ridge formation (RF) in addition to wrinkling and PD modes. The RF mode is favored for small thickness ratios and large pre-stretches, where the PD mode occurs at large thickness ratios and large pre-stretches; no PQ mode is obtained at this strain rate. Comparing the two diagrams, we note that the RF mode is suppressed at a relatively high strain rate, whereas the PD/PQ mode is suppressed at a low strain rate. Previous studies (Cao and Hutchinson, 2012; Zang et al., 2012; R. Zhao et al., 2015; Jin et al., 2015) have suggested that ridge formation requires a relatively large pre-stretch of the substrate in elastic bilayer systems. In the trilayer model, the effect of substrate pre-stretch is significant for the cases with a thin viscoelastic mid-layer, promoting ridge formation (at a low strain rate). In contrast, with a relatively thick viscoelastic mid-layer, the effect of substrate pre-stretch diminishes, hence favoring the transition to the PD/PQ mode. Similar to the elastic bilayers (Cao and Hutchinson, 2012; Y. Zhao et al., 2015; Zhuo and Zhang, 2015), the critical strain for PD increases with increasing pre-stretch, or equivalently by decreasing the thickness ratio (h_v/h_f) in the

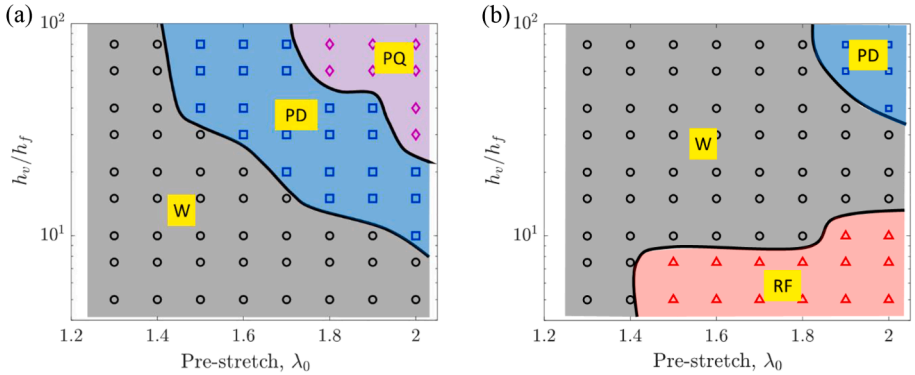

Fig. 13. Bifurcation phase diagrams at the end of compression with different nominal strain rates: (a) $\dot{\epsilon}\tau_v = 1$; (b) $\dot{\epsilon}\tau_v = 0.01$.

trilayer model. In the previous experiments (Chatterjee, et al., 2015), only wrinkling and ridge formation were observed, possibly due to the relatively low strain rates and small thickness ratios, corresponding to the lower part of Fig. 13b.

Fig. 13 shows that the bifurcation phase diagram at the end of the compression step is rate dependent. If the trilayer system is held at the constant nominal strain after compression, the bifurcation mode may continue to evolve over time and eventually reaches an equilibrium state. By holding the trilayer for a long time (up to $10^4\tau_v$), we obtain an equilibrium phase diagram, which is nearly identical for all strain rates. As shown in Fig. 14, three bifurcation modes are observed in the equilibrium phase diagram: wrinkling (W), ridge formation (RF), and periodic folding (PF). In comparison with Fig. 13, we note that wrinkles after compression may stay as wrinkles (with different wavelength and amplitude), or evolve to form either ridges (for small thickness ratios) or folds (for large thickness ratios) after holding. The ridge formation in most cases is stable during holding, but may evolve back to wrinkles in some cases (depending on the ridge aspect ratio A_r/b_r). The PD/PQ modes are unstable upon holding, which may evolve back to wrinkles or form folds (depending on the ratio A_p/A_s). There appears to be an intermediate range for the thickness ratio, within which the wrinkling mode remains stable in equilibrium (after holding), even for the cases of a large pre-stretch (e.g., $\lambda_0 = 2$) and a correspondingly large nominal strain (e.g., $\varepsilon_f = 0.4$). Previous experiments by Auguste et al. (2018) showed that high-aspect-ratio wrinkles could be obtained and stabilized up to a fairly large compressive strain (>0.4) by using an elastic bilayer with relatively small thickness ratios on top of an elastomer mounting layer, essentially an elastic trilayer system similar to the equilibrium state of the trilayer model in the present study. Indeed, they observed ridge formation with a smaller thickness ratio and periodic folding with a larger thickness ratio, qualitatively consistent with the equilibrium bifurcation phase diagram (Fig. 14).

We note that the bifurcation phase diagrams in Figs. 13 and 14 are obtained with a set of particular material parameters in the trilayer model: $\mu_f/\mu_s = 200, \mu_r/\mu_s = 0.02, \mu_g = 10\mu_r$. Different diagrams may be obtained by changing these parameters for different materials. Motivated by the experiments in Chatterjee et al. (2015), we have taken the elastic film to be much stiffer than the viscoelastic layer and the substrate, in which case the first bifurcation mode is always wrinkling. However, if the elastic modulus of the film is comparable to the glassy or rubbery modulus of the viscoelastic layer, other bifurcation modes such as creasing may occur (Wang and Zhao, 2014). Moreover, the viscoelastic property of the mid-layer could be more complicated with multiple time scales as in a typical model for polymer viscoelasticity, which would influence the rate dependence significantly. By assuming a simple viscoelastic material model, the results from the present study may be considered qualitative in general, while more complicated material models should be used for specific material systems. Nevertheless, with a viscoelastic mid-layer in the trilayer model, we show that a variety of bifurcation modes can be obtained by compression and/or holding. Compared to the elastic bilayer systems, the trilayer model offers additional control parameters in terms of the nominal strain rate and the thickness ratio (h_v/h_f), which may enable designing and producing various features of surface morphology for novel applications (Cao et al., 2014; Wang and Zhao, 2016).

5. Summary

Motivated by experiments (Chatterjee, et al., 2015), a trilayer model with a viscoelastic layer between an elastic thin film and a pre-stretched elastomer substrate is used to study the rate-dependent wrinkling and subsequent bifurcations. With a moderate substrate pre-stretch and compressive strain, the only bifurcation mode obtained is wrinkling, with evolution of wrinkle wavelength and amplitude during compression and holding, depending on the nominal strain rate and the thickness of the viscoelastic layer. The rate-dependent wrinkle wavelength can be correlated to the viscoelastic property of the mid-layer in the trilayer system, potentially offering a method to measure the viscoelastic property of a thin polymer layer.

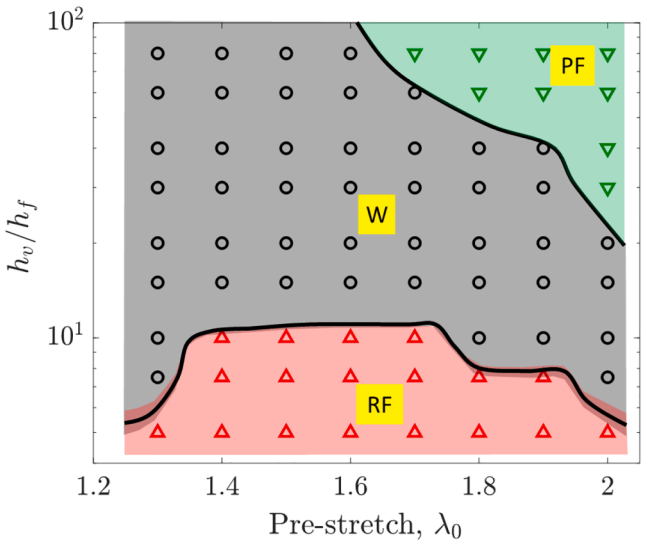

Fig. 14. Equilibrium bifurcation phase diagram obtained after holding the trilayer system for a long time at a constant nominal strain, $\varepsilon_f = (\lambda_0 - 1.2)/\lambda_0$.

With a relatively large substrate pre-stretch and correspondingly a larger compressive strain (up to 0.4), the wrinkles may evolve to other bifurcation modes, depending on the strain rate and the thickness of the mid-layer. Ridge formation occurs when the strain rate is low and the viscoelastic layer is thin. When the ridge growth reaches its limit, more ridges form upon further compression. In contrast, when the strain rate is relatively high and the viscoelastic layer is thick, period-doubling occurs after a critical strain, which may further evolve to period quadrupling and periodic folding by consecutive bifurcations. By varying the substrate pre-stretch and the thickness ratio, bifurcation phase diagrams at the end of compression are constructed for different nominal strain rates. After compression, holding the trilayer at a constant nominal strain allows the surface morphology to evolve over time, eventually reaching an equilibrium state independent of the strain rate during compression. The equilibrium bifurcation phase diagram obtained after holding shows three bifurcation modes: wrinkling, ridge formation, and periodic folding. Interestingly, period doubling appears to be unstable upon holding, which either evolves back to wrinkling or further evolve to period quadrupling and folding at the end. Compared to the elastic bilayer systems in many previous studies, the trilayer model with a viscoelastic mid-layer offers additional control parameters in terms of the nominal strain rate and the thickness ratio to induce various bifurcation modes by compression and/or holding, which may enable designing and producing desired features of surface morphology for novel applications.

Declaration of Competing Interest

The authors declare that they have no known competing financial interests or personal relationships that could have appeared to influence the work reported in this paper.

Acknowledgements

The authors gratefully acknowledge financial support of this work by National Science Foundation through Grant No. CMMI-1562820.

References

Allen, H.G., 1969. Analysis and Design of Sandwich Panels. Pergamon, New York.

Auguste, A., Jin, L., Suo, Z., Hayward, R.C., 2014. The role of substrate pre-stretch in post-wrinkling bifurcations. Soft Matter 10, 6520–6529.

Auguste, A., Yang, J., Jin, L., Chen, D., Suo, Z., Hayward, R.C., 2018. Formation of high aspect ratio wrinkles and ridges on elastic bilayers with small thickness contrast. Soft Matter 14, 8545–8551.

Biot, M.A., 1963. Surface Instability of Rubber in Compression. Appl. Sci. Res. 12, 168–182.

Brau, F., Vandeparre, H., Sabbah, A., Poulard, C., Boudaoud, A., Damman, P., 2011. Multiple-length-scale elastic instability mimics parametric resonance of nonlinear oscillators. Nat. Phys. 7, 56–60.

Brau, F., Damman, P., Diamant, H., Witten, T.A., 2013. Wrinkle to fold transition: influence of the substrate response. Soft Matter 9, 8177–8186.

Budday, S., Kuhl, E., Hutchinson, J.W., 2015. Period-doubling and period-tripling in growing bilayered systems. Philos. Mag. 95, 3208–3224.

Cai, Z.X., Fu, Y.B., 2019. Effects of pre-stretch, compressibility and material constitution on the period-doubling secondary bifurcation of a film/substrate bilayer. Int. J. Non-Linear Mech. 115, 11–19.

Cao, C., Chan, H.F., Zang, J., Leong, K.W., Zhao, X., 2014. Harnessing localized ridges for high-aspect-ratio hierarchical patterns with dynamic tunability and multifunctionality. Adv. Mater. 26, 1763–1770.

Cao, Y., Hutchinson, J.W., 2011. From wrinkles to creases in elastomers: the instability and imperfection-sensitivity of wrinkling. Proc. R. Soc. A 468, 94–115.

Cao, Y., Hutchinson, J.W., 2012. Wrinkling Phenomena in Neo-Hookean Film/Substrate Bilayers. J. Appl. Mech. 79, 031019.

Chan, E.P., Page, K.A., Im, S.H., Patton, D.L., Huang, R., Stafford, C.M., 2009. Viscoelastic properties of confined polymer films measured via thermal wrinkling. Soft Matter 5, 4638–4641.

Chan, E.P., Smit, E.J., Hayward, R.C., Crosby, A.J., 2008. Surface wrinkles for smart adhesion. Adv. Mater. 20, 711–716.

Chatterjee, S., McDonald, C., Niu, J., Velankar, S.S., Wang, P., Huang, R., 2015. Wrinkling and folding of thin film by viscous stress. Soft Matter 11, 1814–1827.

Chung, J.Y., Nolte, A., Stafford, C.M., 2011. A versatile platform for measuring thin-film properties. Adv. Mater. 23, 349–368.

Diab, M., Zhang, T., Zhao, R., Gao, H., Kim, K.-S., 2013. Ruga mechanics of creasing: from instantaneous to setback creases. Proc. R. Soc. A 469, 20120753.

Diab, M., Kim, K.-S., 2014. Ruga-formation instabilities of a graded stiffness boundary layer in a neo-Hookean solid. Proc. R. Soc. A 470, 20140218.

Ebata, Y., Croll, A.B., Crosby, A.J., 2012. Wrinkling and strain localizations in polymer thin films. Soft Matter 8, 9086–9091.

Hohlfeld, E., Mahadevan, L., 2011. Unfolding the sulcus. Phys. Rev. Lett. 106, 105702.

Hong, W., Zhao, X., Suo, Z., 2009. Formation of creases on the surfaces of elastomers and gels. Appl. Phys. Lett. 95, 111901.

Huang, R., 2005. Kinetic wrinkling of an elastic film on a viscoelastic substrate. J. Mech. Phys. Solids 53, 63–89.

Huang, R., Im, S.H., 2006. Dynamics of wrinkle growth and coarsening in stressed thin films. Phys. Rev. E 74, 026214.

Huang, R., Suo, Z., 2002. Wrinkling of a compressed elastic film on a viscous layer. J. Appl. Phys. 91, 1135–1142.

Huang, Z.Y., Hong, W., Suo, Z., 2005. Nonlinear analyses of wrinkles in a film bonded to a compliant substrate. J. Mech. Phys. Solids 53, 2101–2118.

Jiang, H., Khang, D.Y., Song, J., Sun, Y., Huang, Y., Rogers, J.A., 2007. Finite Deformation Mechanics in Buckled Thin Films on Compliant Supports. Proc. Natl. Acad. Sci. 104, 15607–15612.

Jin, L., Takei, A., Hutchinson, J.W., 2015. Mechanics of wrinkle/ridge transitions in thin film/substrate systems. J. Mech. Phys. Solids 81, 22–40.

Jung, J.H., Bae, J., Moon, M.-W., Kim, K.-S., Ihm, J., 2015. Numerical Study on Sequential Period-Doubling Bifurcations of Graphene Wrinkles on a Soft Substrate. Solid State Commun. 222, 14–17.

Khang, D.Y., Jiang, H., Huang, Y., Rogers, J.A., 2006. A Stretchable Form of Single-Crystal Silicon for High-Performance Electronics on Rubber Substrates. Science 311, 208–212.

Liang, J., Huang, R., Yin, H., Sturm, J.C., Hobart, K.D., Suo, Z., 2002. Relaxation of compressed elastic islands on a viscous layer. Acta Materialia 50, 2933–2944.

Lin, P.-C., Vajpayee, S., Jagota, A., Hui, C.-Y., Yang, S., 2008. Mechanically Tunable Dry Adhesive From Wrinkled Elastomers. Soft Matter 4, 1830–1835.

Mei, H., Landis, C.M., Huang, R., 2011. Concomitant wrinkling and buckle-delamination of elastic thin films on compliant substrates. Mech. Mater. 43, 627–642.

Pocivavsek, L., Dellsy, R., Kern, A., Johnson, S., Lin, B., Lee, K.Y.C., Cerda, E., 2008. Stress and fold localization in thin elastic membranes. Science 320, 912–916.

Rahmawan, Y., Moon, M.-W., Kim, K.-S., Lee, K.-R., Suh, K.-Y., 2010. Wrinkled, Dual-Scale Structures of Diamond-Like Carbon (DLC) for Superhydrophobicity. Langmuir 26, 484–491.

Simo, J.C., 1987. On a fully three-dimensional finite-strain viscoelastic damage model: formulation and computational aspects. Comput. Methods Appl. Mech. Eng. 60, 153–173.

Stafford, C.M., Harrison, C., Beers, K.L., Karim, A., Amis, E.J., Vanlandingham, M.R., Kim, H.C., Volksen, W., Miller, R.D., Simonyi, E.E., 2004. A buckling-based metrology for measuring the elastic moduli of polymeric thin films. Nat. Mater. 3, 545–550.

Stafford, C.M., Vogt, B.D., Harrison, C., Julthongpiput, D., Huang, R., 2006. Elastic Moduli of Ultrathin Amorphous Polymer Films. Macromolecules 39, 5095–5099.

Sun, J.-Y., Xia, S., Moon, M.-W., Oh, K., Kim, K.-S., 2012. Folding wrinkles of a thin stiff layer on a soft substrate. Pro. R. Soc. 468, 932–953.

Takei, A., Jin, L., Hutchinson, J.W., Fujita, H., 2014. Ridge localizations and networks in thin films compressed by the incremental release of a large equi-biaxial pre-stretch in the substrate. Adv. Mater. 26, 4061–4067.

Wang, Q., Zhao, X., 2014. Phase diagrams of instabilities in compressed film–substrate systems. J. Appl. Mech. 81, 051004.

Wang, Q., Zhao, X., 2016. Beyond wrinkles: Multimodal surface instabilities for multifunctional patterning. MRS Bull. 41, 115–122.

Xia, Z.C., Hutchinson, J.W., 2000. Crack Patterns in Thin Films. J. Mech. Phys. Solids 48, 1107–1131.

Yang, S., Khare, K., Lin, P.C., 2010. Harnessing Surface Wrinkle Patterns in Soft Matter. Adv. Funct. Mater. 20, 2550–2564.

Zang, J., Zhao, X., Cao, Y., Hutchinson, J.W., 2012. Localized ridge wrinkling of stiff films on compliant substrates. J. Mech. Phys. Solids 60, 1265–1279.

Zhao, R., Zhang, T., Diab, M., Gao, H., Kim, K.-S., 2015a. The primary bilayer ruga-phase diagram I: Localizations in ruga evolution. Extreme Mech. Lett. 4, 76–82.

Zhao, R., Diab, M., Kim, K.-S., 2016. The primary bilayer ruga-phase diagram II: Irreversibility in Ruga Evolution. J. Appl. Mech. 83, 091004.

Zhao, Y., Cao, Y., Hong, W., Khurram Wadee, M., Feng, X.-Q., 2015b. Towards a quantitative understanding of period-doubling wrinkling patterns occurring in film/substrate bilayer systems. Proc. R. Soc. A 471, 20140695.

Zhuo, L., Zhang, Y., 2015. From period-doubling to folding in stiff film/soft substrate system: The role of substrate nonlinearity. Int. J. Non-Linear Mech. 76, 1–7.